Retrieval of Precipitable Water over Land using Near Infrared Satellite Remote Sensing Data

Makoto KUJI[1] and Akihiro Uchiyama[2]
[1] *Nara Women's University, Kita-uoya Nishimachi, Nara, 630-8506, Japan,*
E-mail: makato@ics.nara-wu.ac.jp
[2] *Meteorological Research Institute, Nagamine 1-1, Tsukuba, Ibaraki, 305-0052, Japan*

Abstract
Retrieval of precipitable water (vertically integrated water vapor amount) is proposed using near infrared channels of Global Imager onboard Advanced Earth Observing Satellite-II (GLI / ADEOS-II). The principle of retrieval algorithm is based upon that adopted with Moderate Resolution Imaging Spectroradiometer (MODIS) onboard Earth Observing System (EOS) satellite series. Simulations were carried out with GLI Signal Simulator (GSS) to calculate the radiance ratio between water vapor absorbing bands and non-absorbing bands. As a result, it is found that for the case of high spectral reflectance background (a bright target) such as the land surface, the calibration curves are sensitive to the precipitable water variation. For the case of low albedo background (a dark target) such as the ocean surface, on the contrary, the calibration curve is not very sensitive to its variation under conditions of the large water vapor amount. It turns out that aerosol loading has little influence on the retrieval over a bright target for the aerosol optical thickness less than about 1.0 at 500 nm wavelength. A preliminary analysis of GLI data was also carried out and the retrieved result is discussed. It is also anticipated that simultaneous retrieval of the water vapor amount using GLI data along with other channels will lead to improved accuracy of the determination of surface geophysical properties, such as vegetation, ocean color, and snow and ice, through the better atmospheric correction

1. Introduction

Water vapor is one of typical gas species governing the greenhouse effect. Investigation of water vapor distribution is a clue to understand the radiation budget of earth atmosphere system as well as the global energy and hydrological circulation. Although water vapor is mostly distributed in the lower atmosphere (planetary boundary layer from surface to a few kilometers), the water vapor amount often increases in the middle and upper troposphere accompanying horizontal advection of humid air mass. Thus, precipitable water, (i.e. the vertically integrated water vapor amount) is considered to be the most representative quantity of water vapor amount in the atmosphere.

GLI onboard ADEOS-II is designed to obtain data of both the surface properties (vegetation, ocean color, and snow and ice, etc.) and atmospheric properties (cloud, aerosol, and radiation budget, etc.). In general, atmospheric correction is indispensable when surface geophysical properties are retrieved from satellite remote sensing data. Correction of atmospheric ozone, aerosol, and in particular, water vapor is important for precise retrieval of vegetation conditions and ocean color. In the GLI mission, it is currently planned that the water vapor information is incorporated from the quasi-real-time objective analysis data. Nevertheless, it is desirable to use the water vapor information concurrently obtained with same spatial resolution as other channels. In this context, we study feasibility of using near infrared channels of GLI in the retrieval of precipitable water. The principle of the retrieval algorithm is described in Sec. 2 together with assumptions made in the present simulation. In Sec. 3, results of the simulation are analyzed and discussed. And also preliminary results with GLI data are discussed. Section 4 presents the summary and related future works.

2. Retrieval Algorithm and Simulation

The retrieval algorithm is based upon the radiance ratio method. The similar method was already adopted with MODIS / EOS series, and utilizes the radiance ratio between water vapor absorbing and non-absorbing bands to retrieve the precipitable water. In the MODIS case, 940 nm and 865 nm bands were adopted as the water vapor absorbing band and non-absorbing band [1)], respectively, and the retrieved results on a global scale were already reported [2)].

Principle of the retrieval algorithm is explained concisely here. Figure 1 illustrates transmittance

curves of water vapor in the near infrared region calculated, using the LOWTRAN 7 code [3].

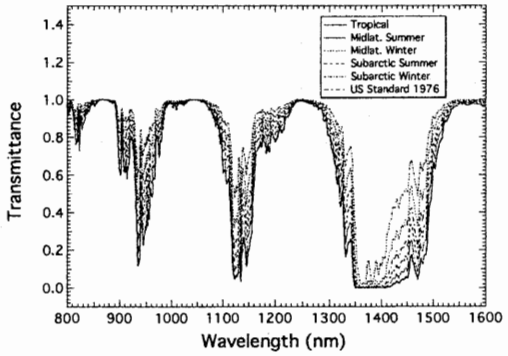

Fig. 1. Atmospheric transmittance related to water vapor in the near infrared spectral region. Curves are calculated with the LOWTRAN 7 code for vertical one way path, as products between water vapor absorption lines and continuum absorption. Each of the six transmittance lines correspond to the six model atmospheres.

As seen from Fig. 1, water vapor absorbing bands (spectral regions with smaller transmittance) are located at around 810 nm, 940 nm, 1135 nm, and 1380 nm, whereas non-absorbing bands (regions with larger transmittance; i.e., atmospheric window region) are found at 865 nm, 1050 nm and 1240 nm. The six atmospheric models are Tropical Atmosphere, Midlatitude Summer, Subarctic Summer, US Standard 1976, Midlatitude Winter and Subarctic Winter and their precipitable water are 40.0 mm, 28.5 mm, 20.4 mm, 13.9 mm, 8.38 mm and 4.10 mm, respectively. The retrieval algorithm utilizes these characteristics as follows: in the water vapor absorbing bands, transmittance (i.e., radiance to be observed) varies with the water vapor amount (precipitable water) assumed in each atmospheric model, while in the non-absorbing bands, changes are much smaller.

It is then proposed that for the GLI application, a retrieval method to make a calibration curve between the radiance ratio of water vapor absorbing band (e.g., Ch. 25; 1135 nm) to non-absorbing band (e.g., Ch. 24; 1050 nm) and water vapor amount (precipitable water) in a form of a nonlinear regressive curve. The GLI channel specifications are summarised in Nakajima et al. [4].

Based upon the principle of the retrieval algorithm, the channel which is most sensitive to variation of water vapor amount is feasible as a water vapor absorption channel and, on the other hand, the one which is least sensitive to it as a non-absorbing channel. As seen from Fig. 1, Ch. 25 (1135 nm; Band Width 70 nm) is selected as a water vapor absorbing channels. For non-absorbing bands, Ch. 24 (1050 nm; Band Width 20 nm) and Ch. 26 (1240 nm; Band Width 20 nm) are selected.

Simulations were carried out with GLI Signal Simulator (GSS) [5] so as to calculate radiances to be observed at the GLI / ADEOS-II. It enables us to calculate the radiance to be observed with GLI assuming several atmospheric models including aerosol loading as well as water vapor. In this feasibility study, two cases of a bright target (land) and a dark target (ocean) are considered as a ground surface condition with the GSS simulations.

The land model is assumed as a Lambertian surface whose spectral reflectance is 50 %, which is adopted as a representative of a bright target. This assumption is based upon the grass model adopted in the ASTER spectral library (http://speclib.jpl.nasa.gov/archive/jhu/becknic/vegetation/txt/grass.txt), which shows surface reflectance is 52.2 %, and 50.7 %, and 48.8 % for 1050 nm, 1135 nm, and 1240 nm spectral region, respectively. Further, the effect of bidirectional reflectance distribution function is not considered in this study for simplicity, too. The ocean model was assumed as a non-Lambertian surface with a flux albedo of around 2 to 6 %, a representative case of a dark target. This assumption corresponds to the situation with 5.0 m s^{-1} wind speed at the 10 m height [6].

Simulations were carried out under clear sky conditions. Moreover, effect of aerosol loading in the model atmosphere was examined. For the aerosol model, rural and oceanic ones incorporated in the GSS are utilized over land and ocean, respectively [5].

3. Results and Discussion

The simulated radiances to be observed were analyzed in two cases: over a bright target (i.e., land) and a dark target (i.e., ocean). Three bands, that is, one water vapor absorbing channel (1135 nm) and

two non-absorbing channels (1240 nm and 1050 nm), were used to carry out the simulations. Two combinations were examined so as to make a calibration curve with a radiance ratio between two channels: (1) a combination of 1135 nm and 1240 nm and (2) a combination of 1135 nm and 1050 nm. In addition, two cases are assumed for scan geometry: (a) solar zenith angle 40°, satellite zenith angle 0° (nadir view), and (b) solar zenith angle 60°, satellite zenith angle 60°, and relative azimuthal angle 90°.

a. Analyses

At first, a radiance ratio (T_w) in this study is defined:

$$T_w(ch1,ch2) \equiv \frac{R_{ch1}}{R_{ch2}}, \tag{1}$$

where $ch1$ indicates a water vapor absorbing channel (e.g., 1135 nm spectral region), at which spectral region radiation undergoes a strong absorption due to water vapor, $ch2$ is a non-absorbing channel (e.g., 1240 nm or 1050 nm spectral region), and R is the radiance simulated with GSS at the top of the atmosphere for the specified channel. This definition becomes equivalent to that of Kaufman and Gao [1] in principle, except for a factor due to some ratio of the extraterritorial solar incident irradiance between specified channels.

Based upon the definition, a relationship (a calibration curve) between radiance ratio (T_w) and precipitable water (W) similar to Kaufman and Gao [1] is proposed:

$$T_w(ch1,ch2) = a + b\exp\left(-c\sqrt{W}\right), \tag{2}$$

where a, b and c are calibration coefficients. Without the coefficient a, this relationship is also equivalent to that of Kaufman and Gao [1] because it takes the factor of the ratio of the solar terrestrial incident irradiance into the calibration coefficient b. The coefficient a is added to take a bias due to little molecular scattering effect into the relationship explicitly.

In order to take the effect of scan geometry into the calibration curve, the precipitable water is converted to the water vapor path. The relationship between precipitable water (W) and water vapor path (W^*) is given as

$$W^* = W\left(\frac{1}{\cos\theta} + \frac{1}{\cos\theta_0}\right), \tag{3}$$

where θ is satellite zenith angle and θ_0 is solar zenith angle. Using W^* instead of W, Eq. (2) is modified as

$$T_w(ch1,ch2) = a^* + b^*\exp\left(-c^*\sqrt{W^*}\right). \tag{4}$$

In following analyses, once the radiance ratios (T_w) are estimated based upon Eq. (1) using the radiances simulated with GSS, then least-squares fit procedures are carried out with Eq. (2) or (4).

b. Results over a Bright Target (Land)

Figure 2 shows relationships between radiance ratio and precipitable water simulated with six atmospheric models in Fig. 1. This is the case with the solar zenith angle of 40° and satellite zenith angle of 0° (nadir view). From Fig. 2, it is found that both R_{1135}/R_{1240} and R_{1135}/R_{1050} are sensitive to the precipitable water, and they are well fitted with the calibration curve of Eq. (2). Root mean square errors (RMSE) for both cases are less than 0.002. These values are much smaller than the order of calibration curves of about 0.1 to 1.0. It is also found that R_{1135}/R_{1240} has greater dynamic range than R_{1135}/R_{1050} as a whole, since simulated R_{1050} is larger than R_{1240} by a few times.

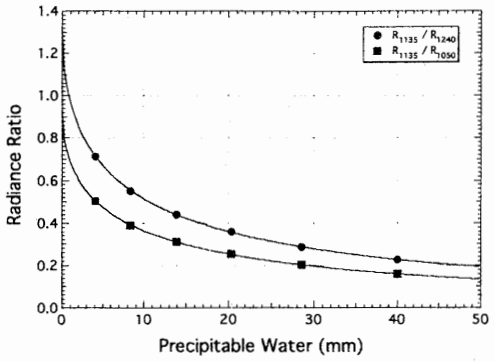

Fig. 2. Radiance ratio simulated as a function of precipitable water over a bright target (land). Closed circles denote the radiance ratio between the 1135 nm and 1240 nm channels, and closed rectangle between the 1135 nm and 1050 nm channels. Solar zenith angle is 40°, satellite zenith angle is 0° (nadir view). Curve fitting is applied to each result to obtain a calibration curve.

Figure 3 shows the radiance ratio calculated for the two cases of the scan geometry; in addition to the case in Fig. 2, results are shown also for solar zenith angle 60°, satellite zenith angle 60°, and relative azimuthal angle 90°. In order to minimize the effect of scan geometry, scaled water vapor path in Eq. (3) is used instead of the precipitable water in Fig. 2. It turns out that all the four cases are well fitted with calibration curves based on Eq. (4) with the RMSEs less than 0.002 for all the four cases. These results indicate that the use of water vapor path enables us to retrieve the precipitable water from the observed radiance ratio irrespective of the scan geometry over bright targets (land surfaces).

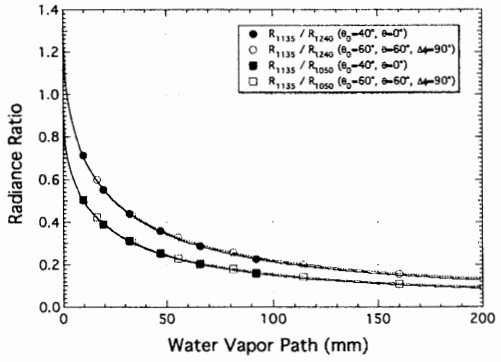

Fig. 3. Calibration curves between the radiance ratio and scaled water vapor path over a bright target (land). Closed and open circles denote the radiance ratio between the 1135 nm and 1240 nm channels, and closed and open rectangles between the 1135 nm and 1050 nm channels. Closed symbols are for the scan geometry of solar zenith angle 40° and satellite zenith angle 0° (nadir view), and open symbols are for solar zenith angle 60°, satellite zenith angle 60°, and relative azimuthal angle 90°. Solid lines are the fitting curves for closed symbols, and dotted lines are for open symbols.

c. Results over a Dark Target (Ocean)

Same as over a bright target (land), simulations were carried out to calculate radiance ratios over a dark target (ocean). Figure 4 shows the radiance ratio calculated for the two cases of the scan geometry; one is a case of solar zenith angle 40° and satellite zenith angle 0° (nadir view), and the other for solar zenith angle 60°, satellite zenith angle 60°, and relative azimuthal angle 90°. In order to minimize the effect of scan geometry, scaled water vapor path in Eq. (3) is also used. It turns that all the four cases are well fitted with calibration curves based upon Eq. (4) and the RMSEs are less than 0.003 for all the four cases. It is also found that the calibration curves are little sensitive to the water vapor amount under a condition of a long water vapor path, that is, larger water vapor amount.

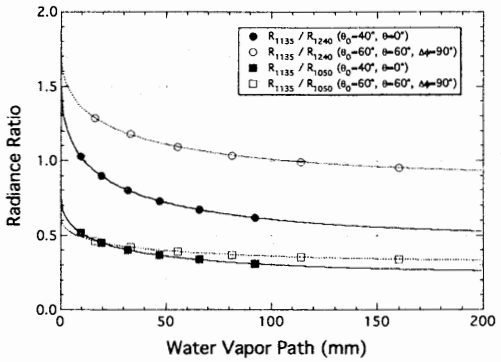

Fig. 4. Same as in Fig. 3, except for over a dark target (ocean).

Over ocean, calibration curves depend upon the scan geometry, which is different from the case over land. That is, ocean surface is not assumed as a Lambertian one in this simulation, although land surface is assumed as a Lambertian one for simplicity in spite of the bidirectional reflectivity in a actual environmental situation. As seen in Fig. 4 compared to Fig. 3, the dynamic ranges of each calibration curve over ocean are smaller than those over land.

d. Effect of Aerosol Loading

Effect of aerosol loading to the retrieval sensitivity in a clear atmosphere was investigated. Simulations with GSS were carried out with the six model atmospheres over both a bright target (land) and a dark target (ocean) changing with aerosol optical thickness at 500 nm (τ_a) of 0.0, 0.1, and 1.0 so as to calculate the radiance ratios.

Figure 5 shows the results of the case over a bright target (land) with rural aerosol loading. From Fig. 5, it is found that all the six cases are fitted well with calibration curve in Eq. (4) and calibration curves are almost identical to each other. The RMSEs are less than 0.002 for all the six cases.

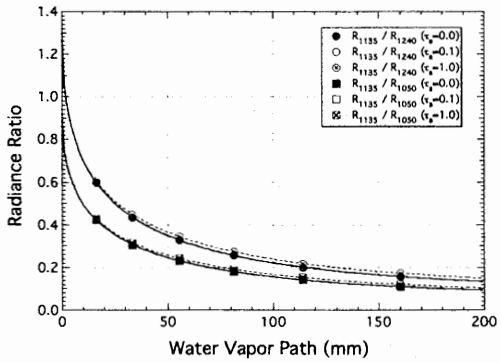

Fig. 5. Same as in Fig. 2, except for rural aerosol loading (τ_a=0.0, 0.1, and 1.0) over a bright target. Circles are used for the radiance ratio between the 1135 nm and 1240 nm channels, and rectangles between the 1135 nm and 1050 nm channels. All the cases are for a scan geometry of solar zenith angle 60°, satellite zenith angle 60°, and relative azimuthal angle 90°.

Figure 6 shows the results of the case over a dark target (ocean) with oceanic aerosol loading. It turns out that all the six cases are fitted well with calibration curves based on Eq. (4) even though the RMSEs are less than 0.01 for all the six cases. The dynamic range of R_{1135}/R_{1240} of calibration curves is larger than that of R_{1135}/R_{1050} because variation of R_{1240} is larger than R_{1050} compared to R_{1135} under this aerosol loading condition. Moreover, the dynamic range of calibration curves also become larger as the aerosol loading is heavier as a whole.

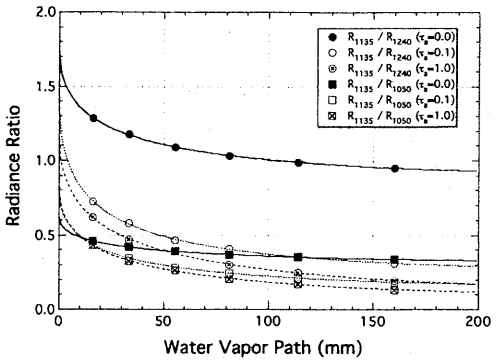

Fig. 6. Same as in Fig. 5, except for oceanic aerosol loading over a dark target.

e. Preliminary analysis of GLI data

The retrieval algorithm described in this study was applied to GLI Data. The data seem to be obtained in a good condition even during the initial checkout as seen in Fig. 7. Figure 7 shows the one of the RGB composite image of ADEOS-II / GLI, which is provided by Japan Aerospace Exploration Agency / Earth Observation Research and application Center (JAXA / EORC). The observation date of the image is March 20, 2003. There extended huge cloud system at the South of Japan. In this panel, there appears western part of Japan islands at the upper part while sunglint region does at the lower part of this panel.

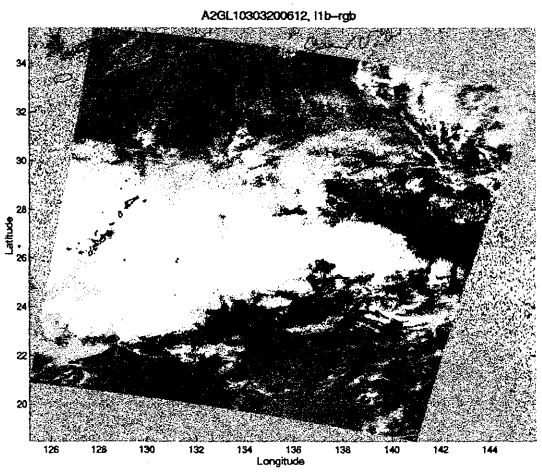

Fig. 7. RGB imagery of GLI data. This imagery is provided by JAXA / EORC.

Figure 8 shows the images of GLI data, same region in Fig. 7, except as a raster format. In Fig. 8, Japan islands locate at the right bottom portion in each panel.

In Fig. 8, panel (b) is strong water vapor absorbing channel, and on the other hand, panels (a) and (c) are non-absorbing (i.e., window) channels. You can see that the sunglint region at the left top corner in the panels (a) and (c) seems to be vague in the panel (b) due to the strong water vapor absorption in the atmosphere.

In this analysis, two channels were utilized such as Ch. 25 (1135nm) and Ch. 26 (1240nm) in the panels (b) and (c), respectively. The three calibration coefficients, a, b, and c for the algorithm in Eq. (2) are assumed as 0.690, 1.23, 0.209, respectively [7]. These coefficients are mainly suitable for land region. So, the retrieved result other than over land will be possibly erroneous. But, the analysis was carried out for the whole scene at this preliminary analysis stage.

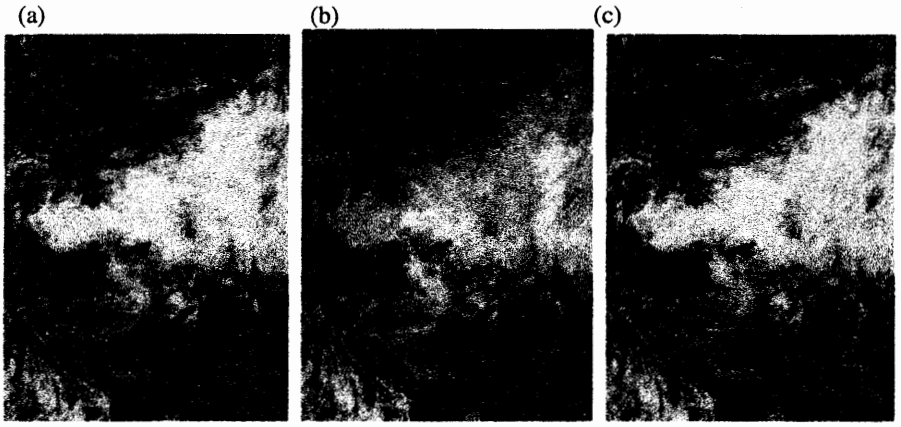

Fig. 8. Images of ADESO-II / GLI data for relevant channels: (a) Ch. 24 (1050nm), (b) Ch. 25 (1135nm), and (c) Ch. 26 (1240nm), respectively. A level slice is a linear gray scale from maximum (white) to minimum (black) radiances for each panel.

Retrieved precipitable water distribution is shown for the whole scene in Fig. 9.

Fig. 9. Retrieved precipitable water distribution. In this preliminary analysis, Ch. 25 (1135nm) and Ch. 26 (1240nm) were used to retrieve precipitable water. A level slice is a linear gray scale from maximum (white) to minimum (black) precipitable water.

As seen in Fig. 9, retrieved precipitable water distributes with great spatial contrast, which increases gradually from bottom (northern) to top (southern) portion. Larger precipitable water in the scene exists around the sunglint region, which is readily interpreted from larger spectral contrast between Fig. 8 (b) and (c). That is, around sunglint region, observed radiance at a non-absorbing channel (Fig. 8 (c)) is brighter, while observed radiance at an absorbing channel (Fig. 8 (b)) is darker in the scene.

Statistics of the retrieved precipitable water distributes averagely 58.4 mm with standard deviation 28.0 mm in the whole scene, which includes not only land region but also ocean and cloudy regions. The retrieved value seems to be much larger than usually observed values around the south of Japan islands region. The retrieved precipitable water should be validated with other observation methods such as radiosonde observation, which is one of the future works.

4. Summary and Concluding Remarks

We have proposed the retrieval of water vapor amount (precipitable water) using GLI near infrared channels. The results of simulations are summarized as follows:

- The combination of 1135 nm and 1240 nm channels is more sensitive to the precipitable water than that of 1135 nm and 1050 nm channels, as a whole.
- The sensitivity to the precipitable water is better over a bright target (higher reflectance at ground level) than over a dark target (lower reflectance at surface level).
- The precipitable water to which radiance ratios are most sensitive is about 5 to 12 mm as a whole, which is rather drier among the six atmospheric models assumed in this study.

- Over a bright target with Lambertian reflectivity, calibration curves using scaled water vapor path are almost independent of the scan geometry.
- Over a dark target with non-Lambertian reflectivity, calibration curves are largely dependent upon the scan geometry even with scaled water vapor path.
- Over a bright target with spectral reflectance of 50 %, aerosol loading with optical thickness not more than 1.0 at 500 nm is not influential in calibration curves.
- Over a dark target with flux albedo of several percent, aerosol loading should be taken into consideration to retrieve precipitable water.

There are further tasks to be worked on in the future:

- Other surface conditions not considered in this simulation should also be examined. It would be required to investigate dependency of calibration curves on scan geometry over land surface such as vegetation, in particular.
- Combined use of non-absorbing channel such as 1050 and 1240 nm channel is expected to improve the retrieval sensitivity, independent of surface reflectance [1)].

Based upon the feasibility study, a preliminary analysis of ADEOS-II / GLI data was carried out. The retrieved water vapor amount is much larger than usually observed values with other observations such as radiosonde and so on. It is necessary to validate the retrieved values, comparing to other observations such as radiosonde, microwave radiometer, and so on, over land region in particular. Further, we hope that in situ observation on surface reflectance specification would be carried out by worldwide researchers in future. At that time, our method to correct water vapor absorption will be supportive for their estimation of surface geophysical parameters over bright targets, in particular. As surface reflectance specification of bright target region will be fulfilled, it is expected that the retrieval of precipitable water will be more accurate vice versa.

Acknowledgments

The authors thank GAIT / EORC / JAXA for simulations with GSS. This study was supported by National Space Development Agency of Japan (A2-RA-G-0030).

References

1) Y. J. Kaufman and B.-C. Gao: Remote Sensing of Water Vapor in the Near IR from EOS/MODIS. *IEEE Trans. Geoscience and Remote Sensing,* **30,** pp. 871-884, 1992.
2) G. -C. Gao and Y. J. Kaufman: Remote sensing of water vapor and thin cirrus clouds using MODIS near-IR channels. *Proc. of SPIE,* **4150,** pp. 217-224, 2000.
3) F. X. Kneizys, E. P. Shettle, L. W. Abreu, J. H. Chetwynd, G. P. Anderson, W. O. Gallery, J. E. A. Selby, and S. A. Clough: Users guide to LOWTRAN 7. **AFGL-TR-88-0177,** 146 pp, 1988.
4) T. Y. Nakajima, T. Nakajima, M. Nakajima, H. Fukushima, M. Kuji, A. Uchiyama, and M. Kishino: The optimization of the Advanced Earth Observing Satellite II Global Imager channels by use of radiative transfer calculations. *Appl. Opt.,* **37,** pp. 3149-3163, 1998.
5) T. Nakajima, T. Y. Nakajima, M. Nakajima, and GLI Algorithm Integration Team (GAIT): Development of ADEOS-II/GLI operational algorithm for earth observation. *Proc. of SPIE,* **3870,** pp. 314-322, 1999.
6) T. Nakajima and M. Tanaka: Effect of wind-generated waves on the transfer of solar radiation in the atmosphere-ocean system. *J. Quant. Spectrosc. Radiat. Transfer,* **29,** pp. 521-537, 1983.
7) M. Kuji and A. Uchiyama: Retrieval of precipitable water using near infrared channels of Global Imager / Advanced Earth Observing Satellite-II (GLI/ADEOS-II). *J. Remote Sens. Soc. Japan,* **22,** 149-162, 2002.